TU Delft

Delft University of Technology

Document Version
Final published version

Licence
Dutch Copyright Act (Article 25fa)

Citation (APA)
Pereira Nunes, J. P., & Seabra, G. S. (2026). Geomechanical Heterogeneity in channelized systems — How much is enough? *Geomechanics for Energy and the Environment*, *45*, Article 100798. https://doi.org/10.1016/j.gete.2026.100798

Important note
To cite this publication, please use the final published version (if applicable).
Please check the document version above.

Copyright
In case the licence states “Dutch Copyright Act (Article 25fa)”, this publication was made available Green Open Access via the TU Delft Institutional Repository pursuant to Dutch Copyright Act (Article 25fa, the Taverne amendment). This provision does not affect copyright ownership.
Unless copyright is transferred by contract or statute, it remains with the copyright holder.

Sharing and reuse
Other than for strictly personal use, it is not permitted to download, forward or distribute the text or part of it, without the consent of the author(s) and/or copyright holder(s), unless the work is under an open content license such as Creative Commons.

Takedown policy
Please contact us and provide details if you believe this document breaches copyrights.
We will remove access to the work immediately and investigate your claim.

This work is downloaded from Delft University of Technology.

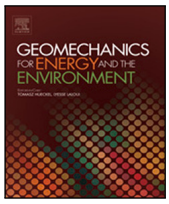
Geomechanics for Energy and the Environment 45 (2026) 100798



Contents lists available at ScienceDirect

Geomechanics for Energy and the Environment

journal homepage: www.elsevier.com/locate/gete



Geomechanical Heterogeneity in channelized systems — How much is enough ?

João Paulo Pereira Nunes [a,*], Gabriel Serrão Seabra [a,b]

[a] Petrobras, Av. Henrique Valadares, 28, Rio de Janeiro, 20231-030, Rio de Janeiro, Brazil
[b] TU Delft, Mekelweg 2, 2628 CD, Delft, The Netherlands

ARTICLE INFO

Editors-in-Chief:
Lyesse Laloui and Tomasz Hueckel

Keywords:
Geomechanical Modeling
Mechanical properties of turbidite systems
Geomechanical upscale
Reservoir modeling

ABSTRACT

The accurate prediction of reservoir compaction and surface subsidence is critical for safe and efficient field development but is often delayed until a detailed reservoir characterization is available. This study investigates whether simplified three-dimensional geomechanical models based on bulk compositional parameters, instead of detailed geological models, can predict compaction and subsidence in channelized sandstone reservoirs. Through direct numerical simulation of an ensemble of synthetic channel systems with varying geometries and facies distribution, and statistical analysis of effective mechanical properties, we demonstrate that shale content is the primary control on the effective Young's modulus of a sand–shale sequence, with the channel geometry having only a minimal impact on the effective modulus. Statistical analysis reveals that a model based primarily on shale fraction can predict effective Young's modulus with high accuracy, while channel geometry parameters contribute to less than 5% to the prediction. Field-scale finite-element simulations confirm that simplified models using bulk shale content produce compaction and subsidence predictions comparable to detailed models with explicit channel representation, while significantly reducing computational and modeling requirements. Our findings enable earlier integration of geomechanical considerations in field development planning by demonstrating that detailed channel characterization, often unavailable in early project stages, is unnecessary for reliable geomechanical predictions.

1. Introduction and motivation

This paper studies if and how the mechanical heterogeneity of a siliciclastic channelized reservoir impacts the predictions of compaction (reservoir thickness decrease) and subsidence (vertical displacement at the seafloor). Reservoir compaction and surface subsidence pose significant challenges to the development and management of hydrocarbon fields. They occur as a result of reservoir depletion during production, which leads to an increase in effective stress that causes the reservoir rock to compact.[1,2]

Production-induced compaction and subsidence have been documented in a wide range of geological settings. Early studies at the Wilmington field demonstrated that thick clastic sequences can undergo severe compaction, prompting decades of research into prediction methods.[2] Geertsma's nucleus-of-strain analytical solution remains a fundamental tool for scenario screening and fast quantitative assessments of surface subsidence,[3] whereas the advent of coupled reservoir–geomechanical simulators has facilitated more advanced and physically consistent predictions of subsidence behavior.[4] Recent syntheses in rock mechanics emphasize the importance of lithology, porosity, and stress-path controls on reservoir deformation.[5] In the North Sea, chalk fields such as Ekofisk and Valhall have experienced significant time-dependent compaction requiring complex elasto-plastic and creep models.[6,7] Also relevant for subsidence studies is the Groningen gas field, which has demonstrated how compaction monitoring through InSAR data can constrain the effective compressibility of the reservoir rocks.[8]

For clastic reservoirs with channelized depositional geometries, such as fluvial or turbidite deposits, the representation of channel geometry in a geomechanical model presents unique challenges due to the inherent heterogeneity of these geological formations and the lack of resolution in the seismic data. Additionally, channel systems are characterized by complex internal architectures that comprise sandstone bodies of varying geometries embedded within a background of finer-grained material (typically shale or mudstone). This heterogeneity creates a composite mechanical system with potentially complex deformation behavior.[9,10]

The conventional approach to geomechanical modeling of heterogeneous reservoirs assumes that a detailed representation of geological

* Corresponding author.
E-mail addresses: jppn@petrobras.com.br (J.P. Pereira Nunes), seabra@petrobras.com.br (G.S. Seabra).

https://doi.org/10.1016/j.gete.2026.100798
Received 24 September 2025; Received in revised form 16 January 2026; Accepted 29 January 2026
Available online 3 February 2026
2352-3808/© 2026 Elsevier Ltd. All rights are reserved, including those for text and data mining, AI training, and similar technologies.

features is necessary for accurate predictions.[4] This assumption may have significant practical implications, postponing a comprehensive geomechanical assessment until the later stages of field development, when a detailed geological characterization is complete and validated through production history. By this time, many critical decisions affecting field architecture, well placement, and facilities design have already been made, often without the benefit of geomechanical insights.

While the impact of geological heterogeneity on fluid flow behavior has been extensively studied, less attention has been paid to whether the same level of detail is required for mechanical behavior prediction, particularly at the field scale where compaction and subsidence are primary concerns.[11] Recently, the issue of geomechanical heterogeneity in carbonate reservoirs has also been explored in the context of CCS.[12] The practical question at the core of this paper is whether the effective mechanical properties of channelized systems, particularly Young's modulus (defined as the ratio of vertical stress to vertical strain in the elastic deformation regime), are controlled primarily by bulk compositional parameters (e.g., shale content), or if the detailed channel geometry (width, thickness, stacking patterns) significantly influences these properties.

This study addresses three key questions: (1) What are the primary controls on the effective mechanical properties in channelized systems?; (2) To what extent does channel geometry influence compaction and subsidence predictions at the field scale?; (3) Can simplified models, based primarily on shale content, deliver reliable results for early field development decisions?

Answering these questions has practical significance for the timing and complexity of geomechanical assessments in early stage field development planning. If detailed channel characterization proves unnecessary for reliable compaction and subsidence prediction, this would enable earlier integration of geomechanical considerations into field development, potentially improving decision-making and risk assessment for operators.

Field evidence of reservoir compaction has been documented in numerous reservoirs, both onshore and offshore. An early example is the Wilmington Field (California), a thick sequence of stacked channels and turbidites that underwent severe compaction during production, causing up to 9 m of surface subsidence by the 1960s.[1] In the offshore context, the North Sea presents the best documented examples. The Valhall and Ekofisk fields, producing from chalk reservoirs (chalk is a very compliant carbonate-like rock), exhibit strong production-induced subsidence. In Ekofisk, a complex jack-up operation was required after the seabed subsided by 10 m.[13]

Our approach involves generating a large set of synthetic channel models with varying geometries and compositions. We calculate their effective mechanical properties, statistically analyze the relationships between model parameters and effective properties, and compare field-scale compaction and subsidence predictions between detailed (heterogeneous) and simplified (homogeneous) models. This systematic approach allows us to explore a wide range of geologically realistic geometries and their corresponding seismic signatures. Thus, highlighting the challenges facing geomodellers in the early stages of field appraisal.

The paper is organized as follows. We start by reviewing the geomechanics of reservoir compaction and the averaging and upscaling of elastic properties. Next, we explain the procedure for the generation of synthetic models of channelized reservoirs and the direct numerical simulation of effective Young's modulus. Then, we introduce the concept of a mechanical Lorenz coefficient and discuss the controls on the Young modulus of a shale-sand sequence. Finally, we present a field-scale case study of a real deep-water turbidite field and explain if and how compaction and subsidence predictions are influenced by the channel's geometry.

2. Geomechanics of compacting reservoirs

Reservoir compaction results from an increase in effective stress as the pore pressure decreases during production.[14] Nowadays, it is common practice for operators to maintain reservoir pressure through water or gas flooding. However, this is rarely achieved in practice, especially in mature fields that have been producing for decades. Reservoir compaction and the resulting land subsidence are common sources of operational failure and environmental hazards.[1] Therefore, the accurate prediction of the onset of compaction is of utmost importance for operators.

In the uniaxial strain conditions typical of extensive reservoir systems, the vertical compaction ($\Delta h/h$, where h represents the original reservoir thickness) can be related to the change in effective vertical stress ($\Delta\sigma'_v$). This relationship, derived from linear poroelasticity theory, can be expressed in terms of Young's modulus (E) and Poisson's ratio (ν) as[15]:

$$\frac{\Delta h}{h} = \frac{(1-2\nu)(1+\nu)}{E(1-\nu)}\Delta\sigma'_v \tag{1}$$

Thus, for a given stress change, the magnitude of compaction is inversely proportional to Young's modulus. The Poisson's ratio is a notoriously difficult parameter to estimate in the laboratory and does not usually display a clear tendency with, for example, porosity.[16] Hence, in most practical applications, it is kept (almost) constant in each lithology of interest. Then, to a first order, we can say that compaction is controlled by the Young's modulus.[1,5,14] Another common way of expressing compaction is through the use of a compaction coefficient (C_m):

$$C_m = \frac{(1-2\nu)(1+\nu)}{E(1-\nu)} \tag{2}$$

Once C_m is known, the vertical strain for any pressure drop is obtained with a single multiplication, which makes the coefficient convenient for rapid field assessments. Geertsma's nucleus-of-strain solution expresses surface subsidence as the convolution of C_m with a Green-function kernel, and this analytic framework has been applied in many producing areas. Early work on the Groningen gas field calibrated C_m values directly from leveling data and used them to forecast future settlement.[3] The same approach is the basis for subsidence management at Ekofisk, where time-lapse seabed surveys are matched by updating a single effective C_m for compacting chalk layers.[17,18] Recent studies on South Pars and other Middle-East gas fields also derive C_m from core tests and wireline logs, then plug it into Geertsma-style kernels to screen casing-shear risk and platform settlement.[19,20] Because the coefficient folds the elastic constants into one parameter, it remains the preferred metric whenever quick, first-order subsidence estimates are needed before detailed finite-element models are available.[21,22]

Beyond core- and log-based methods, modern geodetic techniques have expanded the ways in which C_m can be estimated. Interferometric Synthetic Aperture Radar (InSAR) and GPS networks provide spatially continuous surface deformation measurements that can be inverted for effective reservoir compressibility.[23,24] These methods have been successfully applied in the Groningen field, where multi-decade subsidence records constrain both the magnitude and spatial variability of compaction.[8] Radioactive marker surveys in production wells offer another approach to directly measure reservoir compaction at depth.[25] Unfortunately, none of these methods is applicable to deep-offshore fields, for which there is still a great shortage of direct subsidence measurements.

Model assumptions and scope

The workflow presented in this study is based on several simplifying assumptions that are standard in reservoir geomechanics.[3,5] First, we assume linear poroelastic behavior, meaning that stress–strain relationships remain linear and that deformation is fully recoverable upon

unloading. Second, we adopt the uniaxial strain assumption, whereby lateral deformation is negligible compared to vertical compaction. This assumption is appropriate for laterally extensive reservoirs where the lateral extent greatly exceeds the reservoir thickness.[15]

These assumptions imply that time-dependent (creep) and plastic (irreversible) deformation mechanisms are neglected. Although this constitutes a reasonable simplification for many clastic reservoirs that are maintained under (approximately) constant pressure by water injection and therefore predominantly remain within the elastic regime, it omits key deformation processes occurring in specific geological settings. In particular, chalk reservoirs in the North Sea (e.g., Ekofisk, Valhall) exhibit pronounced creep and pore-collapse behavior, that requires the use of elastoplastic or viscoplastic constitutive formulations.[6,7] However, we should point out that the high levels of compaction observed in these cases were due to inefficient reservoir management practices, which are no longer used today. Similarly, highly compacting formations such as diatomite or poorly consolidated sands may undergo substantial irreversible compaction.[2] The present work is therefore intended for early-stage assessments in the elastic regime and should be complemented by more sophisticated models when significant inelastic behavior is anticipated.[1]

2.1. Young's modulus — Averaging and upscaling

Analytical methods to determine the effective (or upscaled) properties – such as permeability, bulk modulus, and Young's modulus – of a porous material simplify its behavior by focusing on two primary aspects: the material's composition and the distribution and structure of its pores.

In terms of pore geometry, previous studies on homogenization, focusing on elastic properties, have a rich literature in the rock physics community. Eshelby's exact solution for the elastic behavior of an unbounded homogeneous medium with ellipsoidal inclusions[26,27] laid the roots for the development of methods that represent a porous medium as an assembly of idealized pores. This is the origin of the various dilute schemes (i.e., solutions disregarding the interactions between inclusions) that have been proposed to evaluate bulk properties of porous rocks, such as the self-consistent, the differential effective medium, or the Mori–Tanaka approach.[28] In due time, these analytical methods have been employed in micromechanics and rock physics, domains generally associated with scales from millimeters to centimeters. This focus occurred despite the fact that all of these methods are scale-independent. Two possible explanations for the proliferation of such methods are the ease of coding and the cognitive appeal of representing the porous media as an idealized geometry of matrix and inclusions. Unfortunately, this has led to a myriad of, sometimes, confusing and dubious applications that focus on fitting an "effective aspect ratio" to measured or imaged rock samples. However questionable at the micro or core scale, these approaches have not prospered at the field scale, where the rocks are laid with great spatial continuity as a result of geological processes. Consequently, employing idealized random models of non-interacting phases is a much harder sell at the field scale. In this context, the geomechanics community developed analytical models that account for typical reservoir geometries and numerical methods to directly compute the stresses and strains in realistic subsurface conditions.

Aside from the geometry and concentration of pores, another key aspect is the composition of a rock. Numerous studies have demonstrated strong links between lithological composition and stiffness in clastic reservoir rocks. The relationship between shale content and elastic moduli is not straightforward. Shale rocks have a very wide range of elastic behavior, from soft muddy rocks to stiff marls (calcite-rich fine-textured rocks). The literature reflects this complexity, and field and laboratory observations illustrate the composition-stiffness link. In some cases, as shale (clay) volume increases in a sand–shale mixture, the static Young's modulus generally decreases.[29,30] However, in clean channel sands encased in shale-prone overbank deposits, well logs commonly show higher acoustic velocities and dynamic Young's moduli in cleaner sand intervals compared to adjacent shaley zones.

The relationship between acoustic velocity and Young's modulus is fundamental: for a given density, higher compressional velocity implies higher dynamic modulus since $E_{\text{dyn}} \propto \rho V_p^2$. In deep-water turbidite systems, the high-porosity reservoir sands (porosity 25%–30%) are typically characterized by lower velocities (and hence lower moduli) than the surrounding compacted shales.[31] For example, in the Campos basin (Brazil), the turbidite reservoirs display a strong negative reflectivity, resulting from the impedance contrast between high-velocity shales and low-velocity porous sands.[32–34] This negative impedance contrast at the top of the reservoir indicates that the seismic wave travels from a stiffer medium (shale) into a more compliant one (sand). On the other hand, Dou et al.[35] reported that "sandwiched" shales (interbedded thick sand and shale) in the Ordos Basin have a static Young's modulus averaging significantly higher than that of laminated shales with greater mud content. In this work, we consider the case representative of deep-water turbidites: clean, high-porosity reservoir sand (modeled at 5 GPa) encased by compacted, low-porosity shales (modeled at 20 GPa). This choice is consistent with rock physics observations in the Campos Basin and similar deep-water settings.[29,30,35]

Early models treated rock as a two-phase composite and applied bounds or mixing rules, distinguishing clay distributed in laminations (separate shale layers) versus dispersed within sand pores, yielding different effective moduli bounds.[29] Another early example of an analytical solution for a stratified medium was given by Backus[36]. But the simplest and most commonly used alternatives are the Voigt (arithmetic) and Reuss (harmonic) averages, which represent upper and lower bounds for elastic moduli, respectively:

$$E_{Voigt} = \sum_{i=1}^{n} f_i E_i \tag{3}$$

$$\frac{1}{E_{Reuss}} = \sum_{i=1}^{n} \frac{f_i}{E_i} \tag{4}$$

where f_i represents the volume fraction and E_i the Young's modulus of each component i. In laminated stacked formations, the vertical stiffness approaches the Reuss lower bound due to weak layers, whereas dispersed clay yields higher stiffness (closer to the Voigt bound). In the absence of prior information about the geometry, a common assumption is to assume that the effective modulus follows the Voigt–Reuss–Hill average:

$$E_{VRH} = \frac{E_{voigt} + E_{Reuss}}{2} \tag{5}$$

A natural question that arises concerns the applicability of these analytical bounds (or any other method) to channel systems, characterized by more complex geometries. This motivates the use of direct numerical approaches to determine their effective properties.

2.2. Heterogeneity, lithology and compaction

Lithological heterogeneity determines how pressure depletion translates into deformation. In channelized clastic systems, the principal contrast is between stiff, high-porosity sand bodies and the surrounding weaker shale or mudstone. When reservoir pressure declines, the softer phase compacts more than the stiffer one; the resulting differential strain redistributes stress laterally, a process often called stress arching.[2] Where contrasts are large, shear may localize at sand–shale interfaces, potentially damaging well casings or reactivating pre-existing faults.

Laboratory and field studies consistently confirm that deformation localizes in the weaker fraction. Triaxial tests on laminated sand–shale cores show that up to 80% of the axial strain accumulates in the shale layers even when they constitute less than 40% of the total thickness.[29,37] In the Belridge diatomite field, casing-shear failures

occurred where soft siliceous muds compacted next to uncemented channel sands.[2] Time-lapse subsidence surveys in the Groningen gas field likewise revealed local bowls of accelerated settlement where clay-rich intervals are concentrated.[38]

These observations point to practical implications. First, reservoir-scale predictions are governed by the volume fraction of the softer phase because it dictates the composite compliance. As the shale proportion rises, the bulk rock moves rapidly toward the Reuss lower bound, and overall compaction increases non-linearly.[36] Second, Fine-scale geometry matters primarily for local stresses. Detailed mapping of sinuosity, channel stacking or levee pinch-outs is essential when modeling near-well problems (e.g., perforation stability or tubing stresses) but much less so for field-wide estimates of average compaction and seafloor subsidence.[11]

In deep-water developments, three-dimensional seismic is the only data set capable of resolving reservoir architecture; yet conventional streamer surveys rarely image channels thinner than 15–20 m or resolve multi-storey stacking. Because the dominant control on deformation is compositional rather than geometric, the unavoidable seismic "blur" is less detrimental to geomechanical forecasts than to dynamic-flow studies. This observation is related to the hypothesis tested in the present work: can bulk shale content alone predict effective stiffness and, therefore, compaction and subsidence within engineering accuracy?

The next sections quantify this hypothesis using an ensemble of synthetic channel models and field-scale finite-element simulations.

3. Synthetic models of channelized reservoirs — Modeling and simulation

We investigate the relationship between geological heterogeneity and effective mechanical properties in channelized reservoirs via direct simulation of multiple scenarios generated using a dedicated package that mimics geological geometries.[39] The mechanical behavior of each realization is calculated using a high-performance spectral method available in GeoDict.[40] Next, we performed a statistical analysis to identify the primary controls on the effective Young modulus in terms of facies distribution and concentration. Finally, we exemplify an application of our findings to a field-scale simulation comparing predictions from a detailed model with explicit geological features and a homogenized approach.

3.1. The FluvSim package — Channel system generation

FluvSim[39] is utilized for generating scenarios that explore the connection between channel geometries and their effective mechanical properties. FluvSim is an object-based modeling tool specifically designed to generate stochastic realizations of turbidite and fluvial systems.

The FluvSim algorithm operates by generating channel objects as three-dimensional bodies defined by their centerline trajectory and cross-sectional geometry. Each channel centerline is constructed as a sinuous path with user-specified orientation and sinuosity parameters drawn from probability distributions. The cross-sectional template defines the channel shape (typically lenticular or half-elliptical) with width and thickness sampled from input distributions. Channel margin or levee facies can be optionally added as thin zones surrounding the main channel body.[39]

FluvSim uses a process-based approach to model channelized depositional systems, positioning channel objects within a background matrix according to user-defined geometrical and statistical parameters. The software generates channels sequentially, with each new channel potentially eroding previously deposited ones, creating complex stacking patterns and connectivity that mimic natural depositional processes. This erosional stacking rule mimics the natural process of channel avulsion and incision, whereby younger channels cut into and partially remove older deposits. The resulting models exhibit realistic degrees of channel amalgamation and connectivity that depend on the net-to-gross ratio and channel dimensions.

Table 1
Parameter ranges for the FluvSim synthetic channel model realizations.

Parameter	Minimum	Maximum
Channel width (m)	100	200
Channel thickness (m)	5	20
Shale fraction (–)	0.10	0.50

The key parameters that control the channel generation in FluvSim include both geometric variables (width, thickness, and width-to-thickness ratio), patterns (channel sinuosity, which controls the meandering pattern of channels), channel orientation, the stacking pattern, and the net-to-gross ratio (proportion of sand to shale). When conditioning data (e.g., well penetrations) are available, FluvSim can honor these observations by iteratively adjusting channel placement until the specified facies at well locations are reproduced. For the present study, unconditional simulations were used to systematically explore the parameter space without bias from specific well configurations.

To represent a wide range of geological scenarios, we generate 100 different model realizations by systematically varying the channel width, thickness, and shale content within ranges that are representative of typical deep-water turbidite systems. The models have dimensions of 500 × 500 ×100 cells, with a cell size of 1 meter in each direction, resulting in physical dimensions of 500 m ×500 m ×100 m. This scale allows us to capture representative channel geometries and stacking patterns while remaining computationally tractable for the subsequent mechanical property calculations.

To illustrate the limitations of seismic data in resolving detailed channel geometries, we also simulate synthetic seismic responses from selected FluvSim models using a convolutional model with a Ricker wavelet having a 25 Hz dominant frequency, Section 3.3.

3.2. Synthetic models — Parameters and geometry

The FluvSim-generated models span a wide range of channel architectures, from isolated channels in a shale matrix (high shale fraction) to amalgamated, connected channel complexes (low shale fraction). The parameters for the 100 model realizations vary within the ranges specified in Table 1. Later, in Section 3.5, we will introduce the concept of a mechanical Lorenz coefficient to explore whether these parameter ranges fully cover a wide range of possible mechanical behaviors.

Fig. 1 shows the distribution of channel width and thickness across different shale content groups, illustrating the balanced coverage of the parameter space.

Fig. 2 shows examples of generated channel models with varying parameters. The models are visualized in both map view (horizontal slice) and cross-section (vertical slice) to illustrate the three-dimensional nature of the channel geometries. In these visualizations, the channel sand bodies are shown in yellow, channel margin or levee deposits in green, and the background shale in gray.

3.3. Channel geometry and seismic signature

In most practical applications, 3D seismic is the only method available to geoscientists modeling reservoir architecture. However, despite significant advances in recent years, the resolution from conventional streamer-towed seismic is still not enough to provide a detailed picture of complex channel systems. Fig. 3 illustrates the significant loss of detail that may occur in the seismic imaging of channelized systems. In the original FluvSim models, we can observe clear channel boundaries and internal heterogeneities, while in the corresponding synthetic seismic response (right), the channel edges are blurred, and it is not

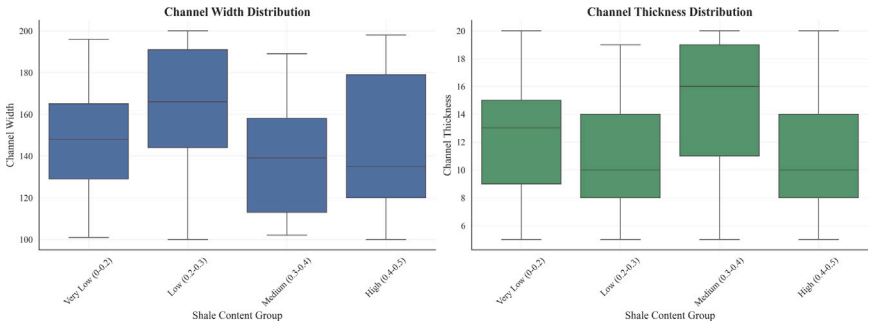


Fig. 1. Distribution of channel dimensions across shale content groups. Left: Channel width distribution. Right: Channel thickness distribution. Shale content groups are defined as Very Low (0–0.2), Low (0.2–0.3), Medium (0.3–0.4) and High (0.4–0.5).

possible to resolve thinner channels or detailed internal structures. The seismic images are generated using a convolutional model[41] with a Ricker wavelet of dominant frequency of 25 Hz, which is typical of a high-quality marine survey in the turbidite reservoirs of the Campos Basin.[32] The Widess criterion stipulates that the vertical seismic resolution can be estimated as one quarter of the wavelength of the seismic pulse: $\lambda = v_p/f_d$,[41] where v_p is the seismic velocity and f_d is the dominant frequency. For the Campos Basin, this results in a typical vertical seismic resolution of 30 m at reservoir depths. The top of the reservoir corresponds to the white peaks in the seismic[32,34]; this is due to the negative impedance contrast between the shale and the sand (Table 2). The seismic wave is moving from a high velocity rock into a low velocity reservoir. As the number of channels increases, the continuity of the seismic signal is compromised. This visualization underscores one of the key motivations for our study: in early-stage reservoir characterization, detailed information about channel geometries is often unavailable or highly uncertain due to seismic resolution limitations.

It is important to note that seismic resolution is fundamentally limited by the physics of wave propagation and does not improve significantly as a field matures. Considering typical values of velocity and reservoir depths between 2000 and 3000 m, the conventional streamer-towed seismic surveys have vertical resolution of approximately 20–30 m, regardless of the project stage. What does improve over time is not resolution per se, but rather the integration of seismic data with well logs, core measurements, and production data, as well as potential reprocessing or quantitative inversion that can better constrain subsurface properties.[41] This observation supports our central argument: since detailed channel geometries remain poorly constrained by seismic data throughout field life, geomechanical predictions should rely on bulk properties (such as shale fraction) that can be reliably estimated from available data rather than on geometric details that remain uncertain.

3.4. Direct numerical simulation of effective moduli

For each synthetic model realization, we calculate the effective Young's modulus by solving the elasticity equations via a spectral method implemented in Geodict.[40,42] For the computation of effective properties, GeoDict solves the linearized elasticity equations:

$$\nabla \cdot \boldsymbol{\sigma} = \mathbf{0} \tag{6}$$

$$\boldsymbol{\sigma} = \mathbb{C} : \boldsymbol{\varepsilon} \tag{7}$$

$$\boldsymbol{\varepsilon} = \frac{1}{2}(\nabla \mathbf{u} + (\nabla \mathbf{u})^T) \tag{8}$$

where $\boldsymbol{\sigma}$ is the stress tensor, $\mathbb{C}$ is the fourth-order stiffness tensor, $\boldsymbol{\varepsilon}$ is the strain tensor, and $\mathbf{u}$ is the displacement vector. Each material is parametrized in terms of its density, porosity, Young's modulus, and Poisson's ratio, and Eqs. (6)–(8) are solved for the entire domain, which deforms as a consequence of the applied external strain. The boundary conditions are consistent with uniaxial strain compaction, which is typical of reservoir settings where lateral deformation is constrained by the surrounding rock. The computational domain encompasses the entire channel system to capture its heterogeneity. The input mechanical properties for the calculations are based on typical values for sandstone and shale rocks in deep-water systems, Table 2. These values are consistent with the mechanical contrast typically observed between sand and shale facies in deep-water clastic systems. For our study, the precise values are less important than their relative difference, since our purpose is to determine which geometric factors influence the effective properties. This negative contrast between the shaly caprock and the sandstone reservoir results in a seismic signature that is a negative peak at the top of the reservoir, see Section 3.3.

Table 2
Mechanical properties of each reservoir facies.[5]

Facies	Young's modulus (GPa)	Poisson's ratio	Density (kg/m^3)
Channel	5	0.25	2400
Channel bank	10	0.25	2500
Shale (background)	20	0.25	2300

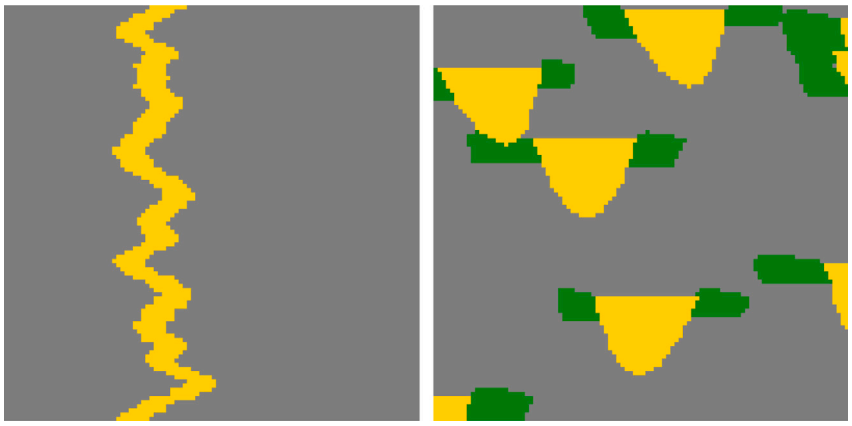
The mechanical property values in Table 2 warrant further discussion. The channel sand modulus of 5 GPa represents a soft, high-porosity (25%–30%) unconsolidated to weakly cemented sand typical of deep-water turbidite reservoirs.[29,31] The shale modulus of 20 GPa represents compacted, low-porosity overbank and hemipelagic deposits. This 4:1 contrast is consistent with rock physics observations in the Campos Basin and similar settings.[30,35] The channel bank (levee) deposits have intermediate properties reflecting their mixed lithology.

The key control on the effective modulus is the contrast between phases and their volume fractions, rather than the absolute values. According to effective medium theory, if all moduli were scaled by a constant factor (e.g., doubling both sand and shale values), the shale-fraction dependence would be preserved, though the absolute E_{eff} values would shift accordingly.[36,43] Our principal conclusion – that shale fraction dominates over channel geometry – remains valid as long as a significant stiffness contrast exists between the channel fill and background facies.

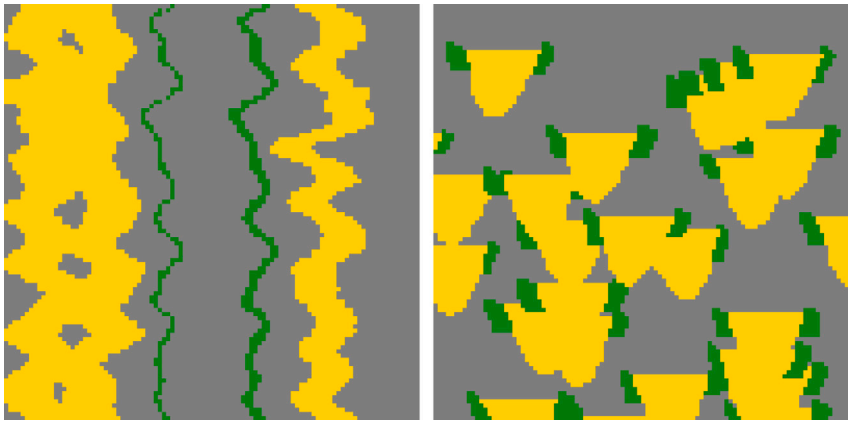
It should be noted that we restrict our investigation of homogenization and upscaling of Young's modulus to the limit of elastic deformations only. Plasticity, rupture, and pore collapse, albeit important in near-field conditions, are rarely relevant to field-scale applications – with the remarkable exception of the highly compressible North Sea chalk reservoirs[1] – therefore, they are not considered here.

3.4.1. Effective Young's modulus

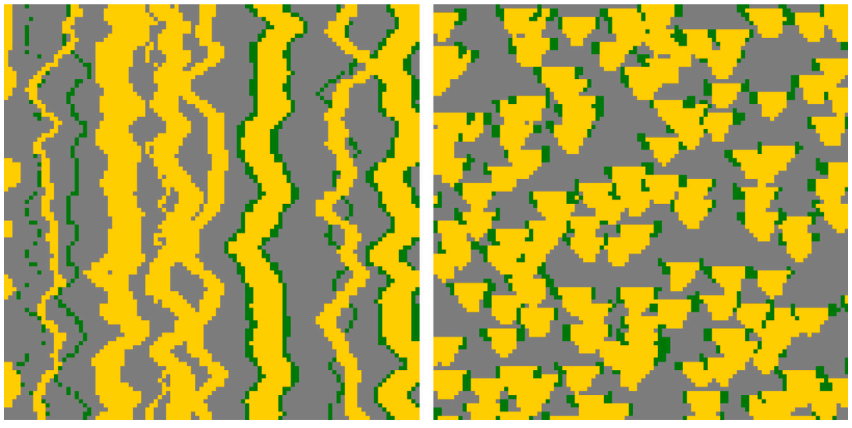
The effective Young's modulus (E_{eff}) is defined as the upscaled, volume-averaged vertical stiffness of the composite reservoir. Mathematically, it is the ratio of the volume-averaged vertical stress ($\langle \sigma_{zz} \rangle$)



(a) Low sand content



(b) Medium sand content



(c) High sand content

Fig. 2. Examples of FluvSim-generated channel models with varying parameters, map view on the left and vertical slice on the right. (a) Model with low sand fraction showing dispersed channel bodies. (b) Model with medium sand fraction showing partially connected channels. (c) Model with high sand fraction showing amalgamated channel bodies. The models are 500 m wide and 100 m deep.

to the volume-averaged vertical strain ($\langle \varepsilon_{zz} \rangle$) under uniaxial strain loading conditions:

$$E_{\text{eff}} = \frac{\langle \sigma_{zz} \rangle}{\langle \varepsilon_{zz} \rangle} \tag{9}$$

This definition follows standard homogenization procedures for elastic composites.[36,43] The "forcing" used in the numerical simulations consists of an imposed macroscopic uniaxial strain boundary condition (vertical displacement at the top boundary with fixed lateral boundaries), which is consistent with reservoir compaction conditions. There is no arbitrary forcing factor; the effective modulus emerges directly from the ratio of computed average stress to applied average strain.

The effective Young's modulus calculated for the ensemble of channel models varies from approximately 9 GPa to 15.5 GPa. Fig. 4 shows an example of a numerical simulation for one of the channel models, illustrating the strain distribution under uniaxial compression.

In Fig. 5, we further illustrate the expected seismic and strain signatures in the models with varying channel thickness and width. The top row shows a highly channelized model: it is challenging to individualize the sand bodies in the seismic data, while the bottom row

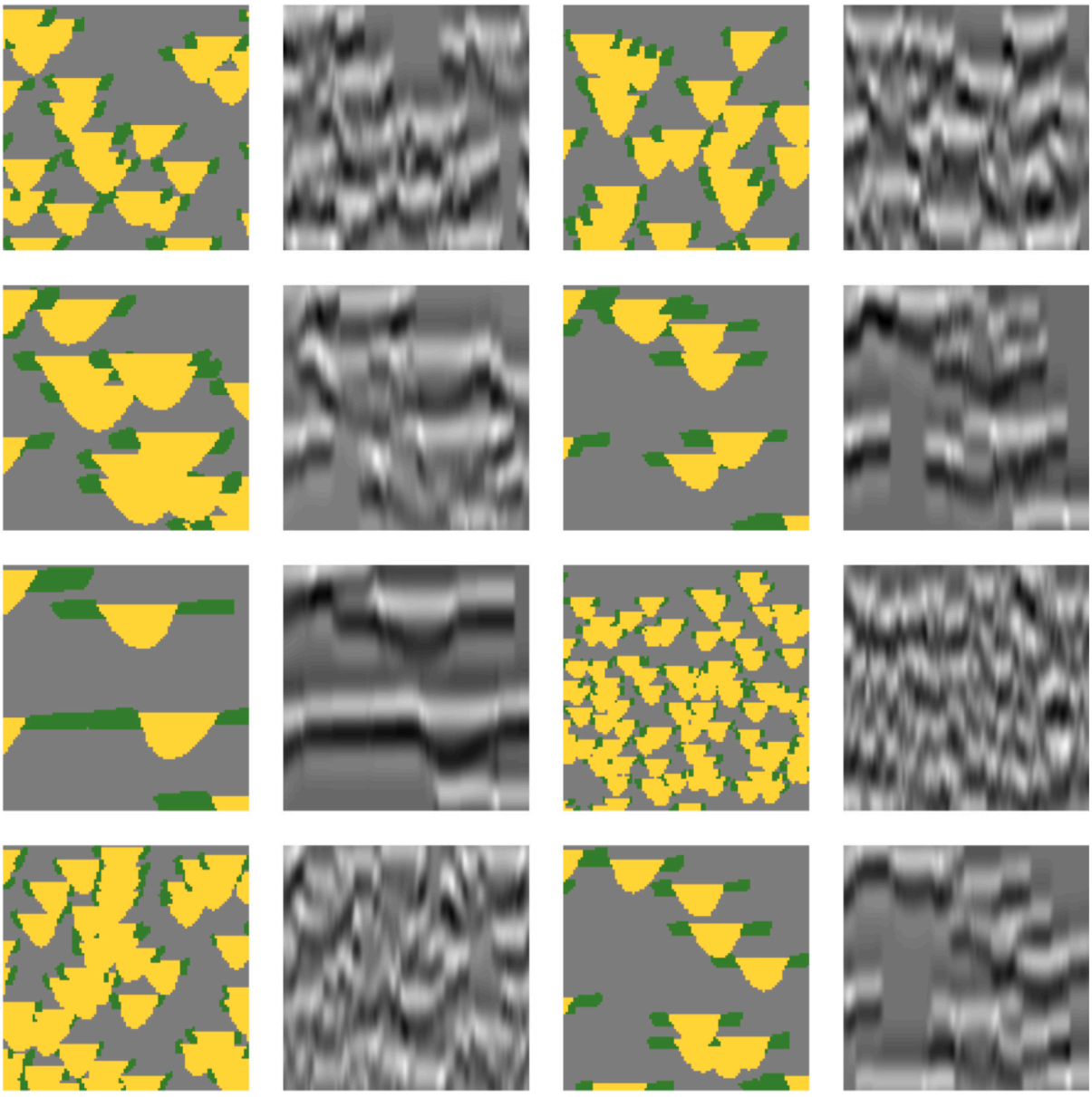


Fig. 3. Subset of the first eight FluvSim models (shale in gray, sand in yellow and spills in green) and the corresponding synthetic seismic. There is a significant loss of detail in the seismic image, where individual channel boundaries are blurred and thinner channels are undistinguishable. White peaks correspond to negative impedance contrasts.

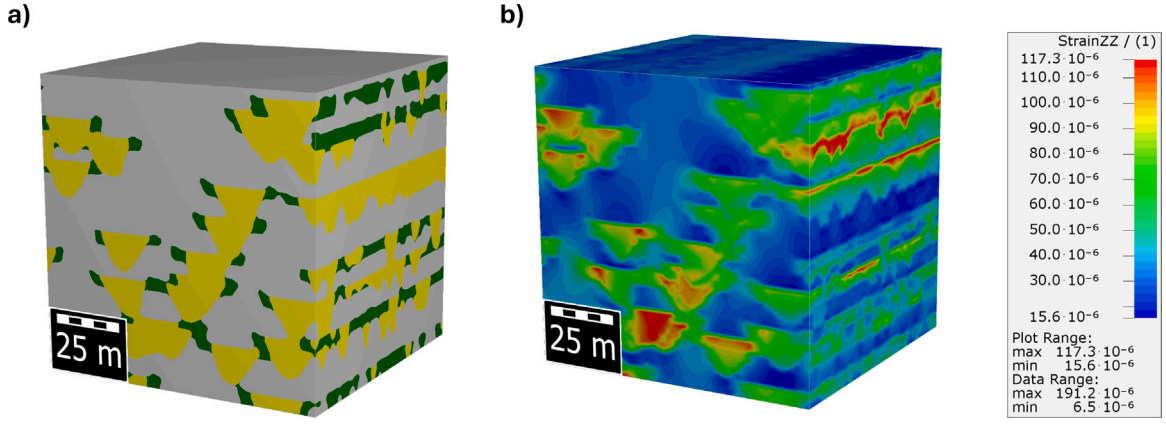


Fig. 4. Example of an elastic simulation: (a) Input facies model from FluvSim, (b) Vertical strain (ϵ_{zz}) under uniaxial compression, showing strain concentration in the softer sand bodies.

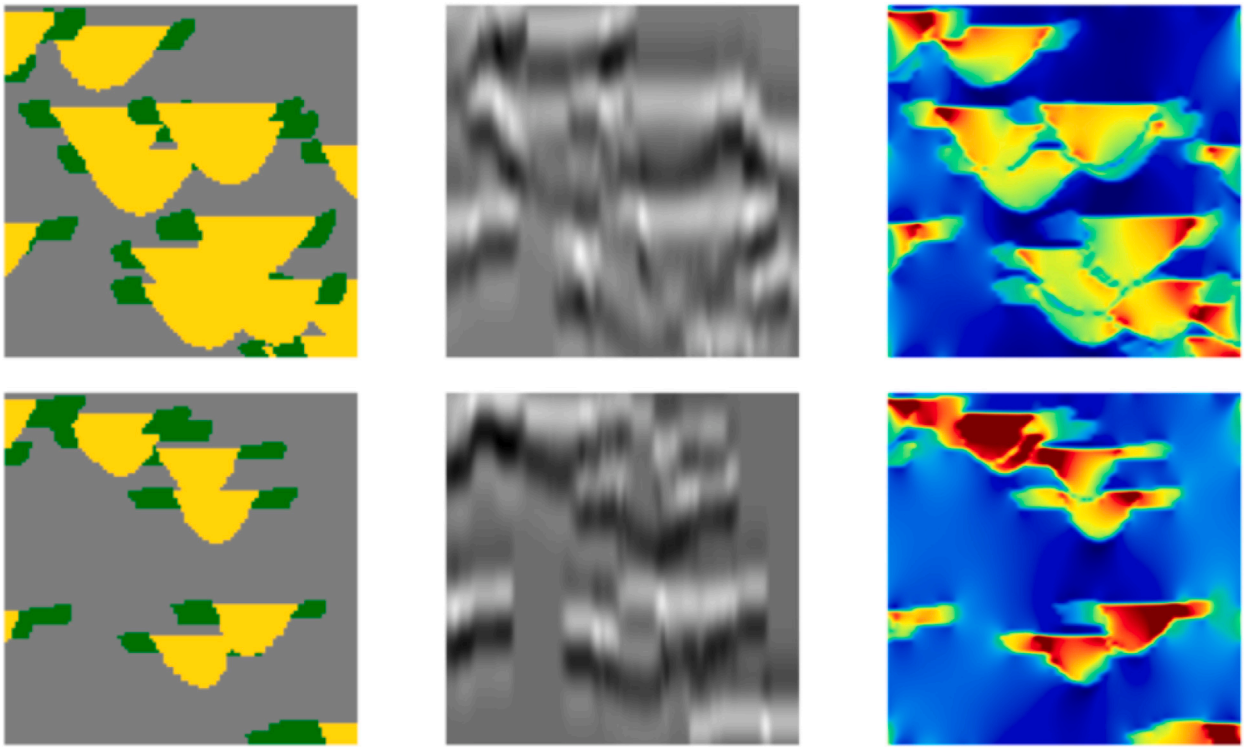


Fig. 5. Two model realizations highlighting their corresponding seismic signatures and strain distributions (rightmost column). In the top model, the channels are not distinguishable in the seismic. In both realizations, we observe strain localization within the sand bodies.

shows a model with a similar sand volume, but where the channels are thicker and easier to map.

Fig. 6 shows the relationship between shale fraction and effective Young's modulus for all 100 models, revealing a strong positive correlation. This positive correlation is physically consistent: shale is modeled as the stiffer phase (20 GPa) and sand as the more compliant phase (5 GPa), reflecting the rock physics of deep-water turbidites where high-porosity channel sands are softer than the surrounding compacted shales. As the shale fraction increases, the composite stiffness increases because a greater proportion of the volume is occupied by the stiffer phase.[29,30]

To assess robustness and allow for non-linear interactions, we also trained a random-forest regressor[44,45]: 200 trees, scikit-learn[46] with default split criteria. The model performance was evaluated using 5-fold cross-validation with the coefficient of determination on the held-out fold as the score. The average across folds is $\bar{R}^2 = 0.955$ with a standard deviation of 0.026, which is consistent with the linear model fit shown in Fig. 6. We also report each feature's importance in two complementary ways. First, the built-in "mean decrease in impurity" (MDI)[47] importance shows V_{sh} contributing about 0.95 of the total, with T and W each around 0.02 (Fig. 7).

Using ordinary least squares regression on the GeoDict simulation results, we derived a predictive equation for the effective Young's modulus E_{eff} (in GPa). The predictor variables are: shale volume fraction (V_{sh}), channel width (W, in meters), and channel thickness (T, in meters). The sample means are $\bar{W}$=144.1 m and $\bar{T}$=12.4 m. The regression equation is:

$$E_{eff} = 2.809 + 15.64\,V_{sh} - 0.0094\,(W - \bar{W}) - 0.0354\,(T - \bar{T}), \tag{10}$$

where the terms $(W-\bar{W})$ and $(T-\bar{T})$ represent deviations from the sample means (mean-centering). The intercept of 2.809 GPa corresponds to an extrapolation to hypothetical pure sand conditions (V_{sh}=0), which lie outside our dataset where shale volume fraction ranges from 0.41 to 0.80.

Coefficient interpretation is direct: a width of 10 m above $\bar{W}$ changes E_{eff} by $-0.0094\times10 = -0.094$ GPa (holding other terms fixed); a thickness of 2 m above $\bar{T}$ changes E_{eff} by $-0.0354\times2 = -0.071$ GPa. The shale slope +15.64 reflects the contrast between the stiff shale matrix (20 GPa) and the soft sand channels (5 GPa), where an increase of 0.1 in V_{sh} raises E_{eff} by about 1.56 GPa at mean geometry. This positive correlation is physically consistent with increasing proportions of the stiffer shale phase dominating the composite behavior.

To visualize these trends directly, Fig. 8 presents a scatter-matrix plot of all variables. The strong positive correlation between shale fraction and modulus stands out, whereas the point clouds involving channel width or thickness are diffuse, confirming their weak effect.

Because the geometric terms are so small, they can often be dropped without losing practical accuracy, resulting in the simpler rule:

$$E_{eff}\ (\text{GPa}) \approx 2.809 + 15.6\,V_{sh} \tag{11}$$

which keeps the error around 0.5 GPa (about 2% of the full range) for all realizations and is adequate for field-scale compaction studies. This simplified relationship captures the essential physics: effective stiffness is primarily controlled by the volume fraction of the stiff shale phase within the studied range (41%–80% shale content).

3.5. A Lorenz plot for mechanical heterogeneity

The Lorenz plot (and the associated Lorenz coefficient) is a common tool employed in petrophysics and formation evaluation to assess the level of flow heterogeneity along a well path.[48] It was originally proposed as a way to describe the wealth or income distribution in a given population.[49] Later, it was presented as a useful diagnostic plot in reservoir engineering,[50] where it has proven to be a fast technique to rank and compare the contribution to total flow from each producing interval; that is, each rock layer is assigned a weight according to its flow capacity, and the Lorenz curve measures how much the flow pattern deviates from an idealized case of uniform flow. To calculate the Lorenz curve of a stacked reservoir comprised of n layers of thickness

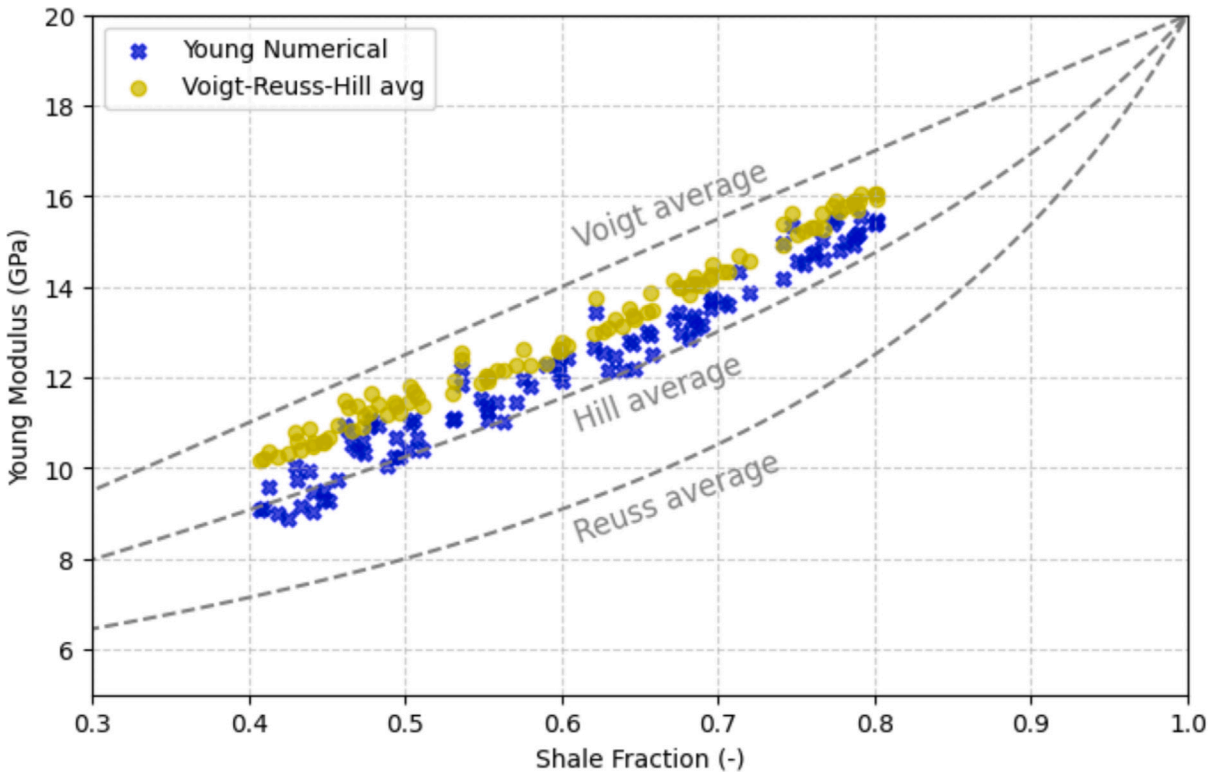


Fig. 6. Relationship between shale fraction and Young's modulus for the 100 synthetic channel models. The strong positive correlation ($R^2 = 0.93$) demonstrates that shale content is the primary control on effective stiffness. For reference the Voigt, Reuss and Voigt–Reuss–Hill averages (Eqs. (3)–(5)) are also plotted.

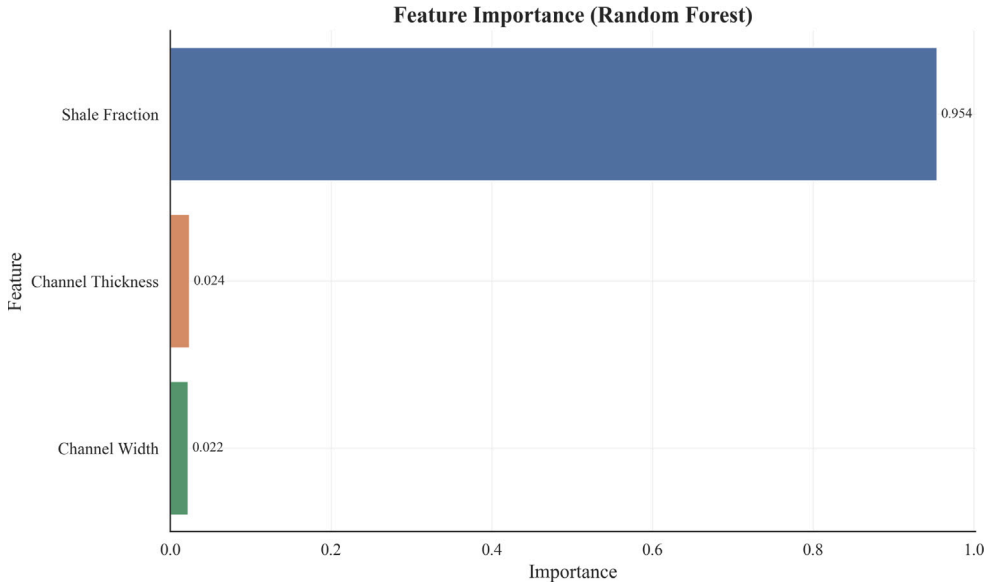


Fig. 7. Random-forest feature importance from the repository run. Shale fraction dominates the prediction of effective Young's modulus, while channel width and thickness have only a minor influence (<5% combined).

h_i, we first rank the corresponding permeability (k_i) and porosity (ϕ_i) data in decreasing order. These usually come from well logs or well tests. Next, we calculate the normalized cumulative flow capacity F:

$$F = \frac{\sum_{i=1}^{m} k_i h_i}{\sum_{i=1}^{n} k_i h_i} \tag{12}$$

where $m = 1, \ldots, n$ and the normalized storage capacity Φ:

$$\Phi = \frac{\sum_{i=1}^{m} \phi_i h_i}{\sum_{i=1}^{n} \phi_i h_i} \tag{13}$$

The deviation of the curve $F(\Phi)$ from the identity line represents the heterogeneity of the system, and the area under it is the Lorenz coefficient.[48,50]

We adapt the Lorenz plot to the context of mechanical heterogeneity by replacing the permeability with the strain and the porosity with the sand fraction, thus defining a normalized strain capacity (analogous to F, Eq. (12)):

$$S = \frac{\sum_{i=1}^{m} \epsilon_i^z h_i}{\sum_{i=1}^{n} \epsilon_i^z h_i} \tag{14}$$

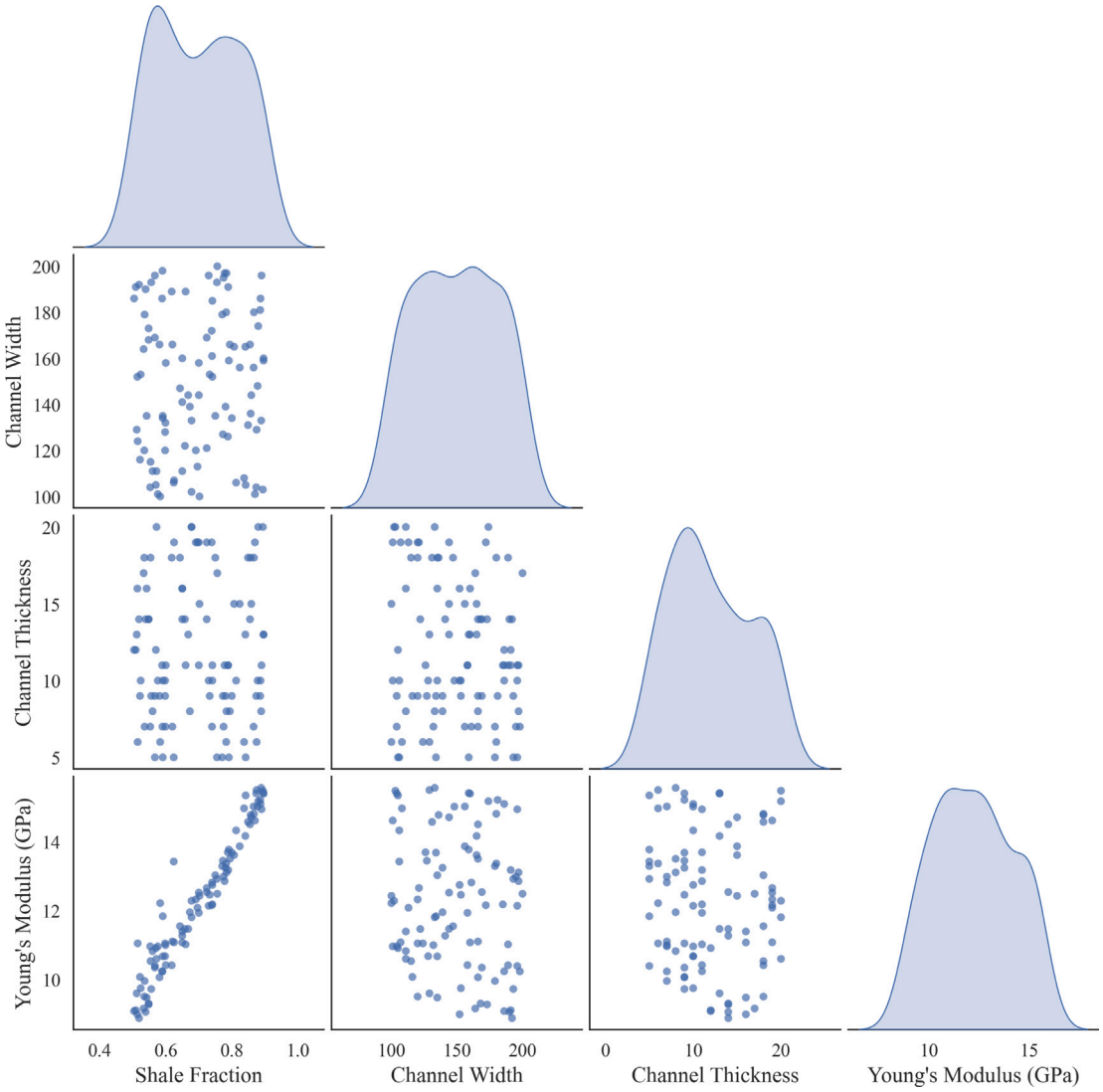


Fig. 8. Scatter-matrix showing pairwise relationships among shale fraction, channel width, channel thickness and Young's modulus. Only shale fraction displays a marked trend with stiffness; channel geometry shows diffuse clouds, consistent with a weak effect.

and a normalized sand volume fraction (analogous to Φ, Eq. (13)):

$$V_{sand} = \frac{\sum_{i=1}^{m} v_i h_i}{\sum_{i=1}^{n} v_i h_i} \tag{15}$$

In a three-dimensional model, the vertical strain (ϵ^z, Eq. (14)) is calculated as the average of each horizontal i layer and ranked in decreasing order vertically. The volume of sand (v, Eq. (15) is defined similarly. The idea is that sand-rich layers compact more and, of course, concentrate strain. We perform this calculation for each model realization, thus graphically representing how the sand distribution contributes to the total reservoir strain and quantifying whether the models have a different overall mechanical behavior.

Models with more sand tend to be more homogeneous, in the sense that they display lower strain concentration (again, the analogous of flow capacity in petrophysics). This is clearly seen in the Lorenz curves being closer to the unity line in Fig. 9. Another way of visualizing the impact of model heterogeneity is to plot the Lorenz coefficient, see Fig. 9, which clearly shows a tendency of increasing Lorenz coefficient as the shale fraction increases. The variation range of the Lorenz coefficient gives us confidence that there is significant mechanical heterogeneity within our model ensemble.

4. The impact of mechanical heterogeneity on field-scale compaction and subsidence

This section presents the application of our findings to the case of a deep-water turbidite oil field. We perform a comparative analysis between heterogeneous and homogeneous geomechanical models, with particular emphasis on compaction and subsidence predictions.

4.1. Geomechanical modeling of a deep-water turbidite

The model represents a deep-water turbidite reservoir bearing 29 API oil and producing via waterflood. The reservoir is a sand–shale sequence, with thickness varying between 100 and 300 m; the average porosity is 26% and the permeability is above 1D. The model has dimensions of 20 km ×20 km and is discretized in a 202 × 194 × 536 regular grid with cell dimensions of 100 × 100 × 10 m. Due to an injection deficit, the reservoir experienced a period of compaction, which is captured by the geomechanical model. This is the focus of this section. The field-scale simulations are performed in GeomecBR, the Petrobras in-house finite element simulator.[51] GeomecBR is a very efficient geomechanical simulator that runs coupled to standard flow simulators and is capable of dealing with highly heterogeneous models

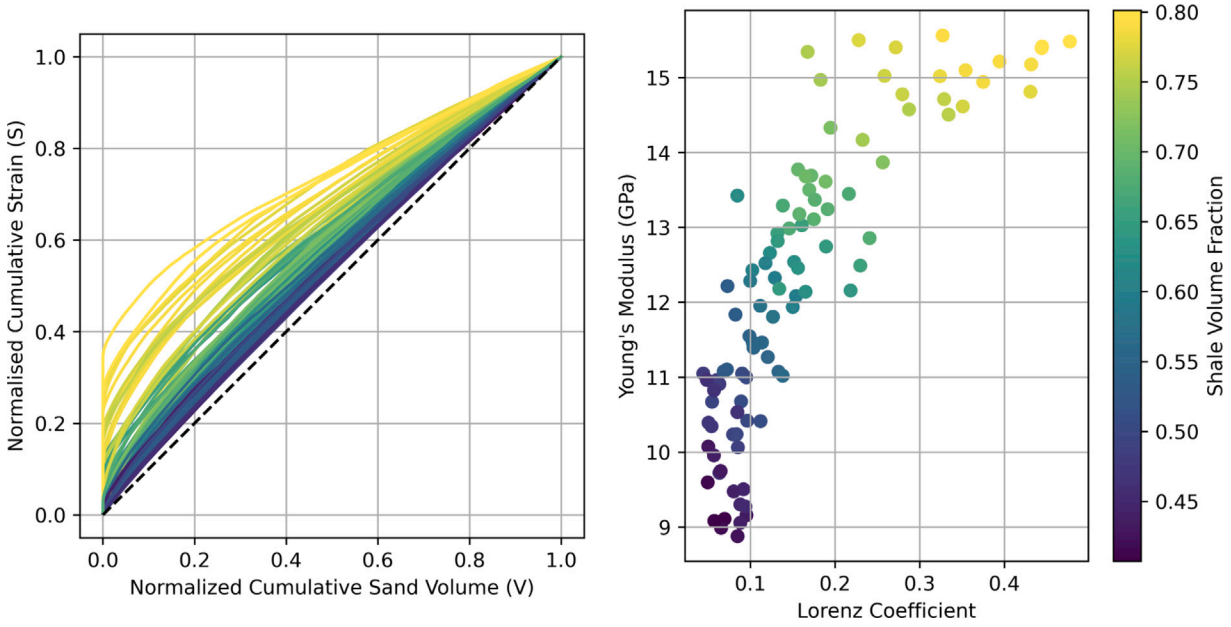


Fig. 9. On the left, a mechanical Lorenz plot, representing the cumulative strain (S) versus the sand volume fraction (V). Each curve represents one channel model. On the right, the Lorenz coefficient versus the effective Young's modulus and colored by the shale fraction.

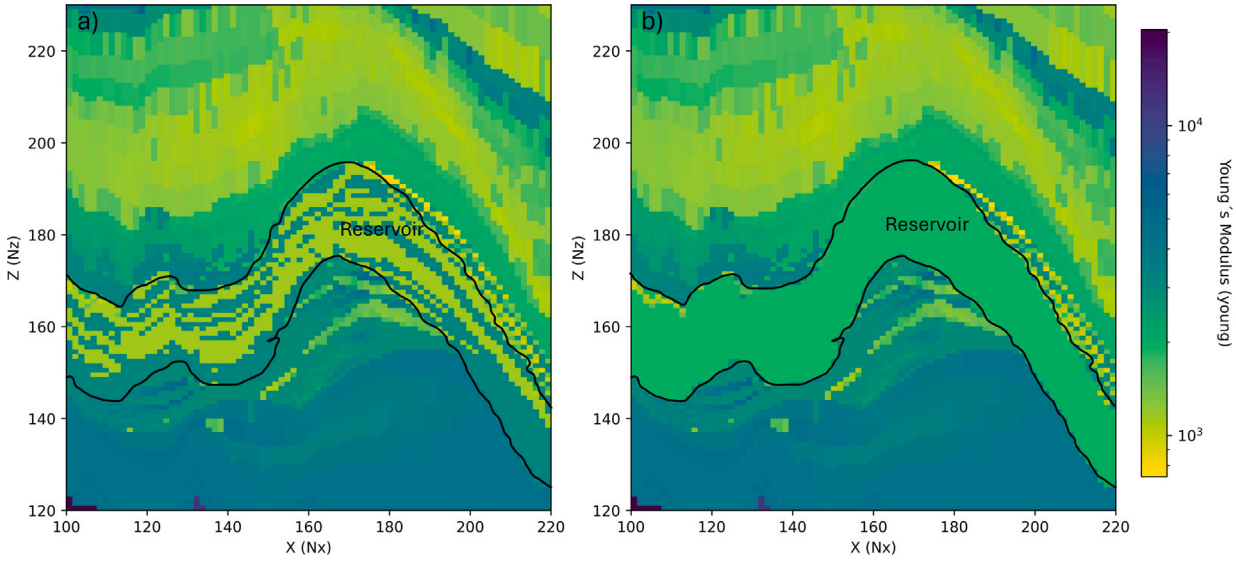


Fig. 10. Vertical cross-section through the central part of the reservoir showing the Young's modulus for the detailed (a) and simplified (b) models. In the simplified representation (b), the finely layered sandshale succession of the detailed model (a) is substituted by a single unit characterized by an averaged Youngs modulus value.

with over 10^8 elements.[12] To simulate production-induced compaction, we apply pore pressure changes representative of typical field depletion scenarios, with maximum depletion reaching 20 MPa after 10 years of production. We compare two different approaches for representing the reservoir interval. In the first case, the model explicitly represents channel geometries, with mechanical properties (Young's modulus and Poisson's ratio) assigned to each facies – sand or shale – Table 2. This is termed the detailed or heterogeneous model. In the second approach, the entire reservoir unit is represented by a single facies with bulk properties derived from the shale content, and the effective Young's modulus is calculated according to Eq. (11), as suggested in Section 3.4.1. This is the simplified or homogeneous model, Fig. 10.

4.2. Compaction and subsidence — Homogeneous and heterogeneous models

Figs. 11 and 12 compare the vertical displacement predictions between the detailed and simplified modeling approaches. The detailed model explicitly represents the channel geometries with different mechanical properties assigned to each facies type, while the simplified model uses bulk properties derived from shale content based on the regression equation developed from our statistical analysis. The results show that the simplified model produces compaction and subsidence predictions that are remarkably similar to those from the detailed model, with differences typically less than 10%. These differences are

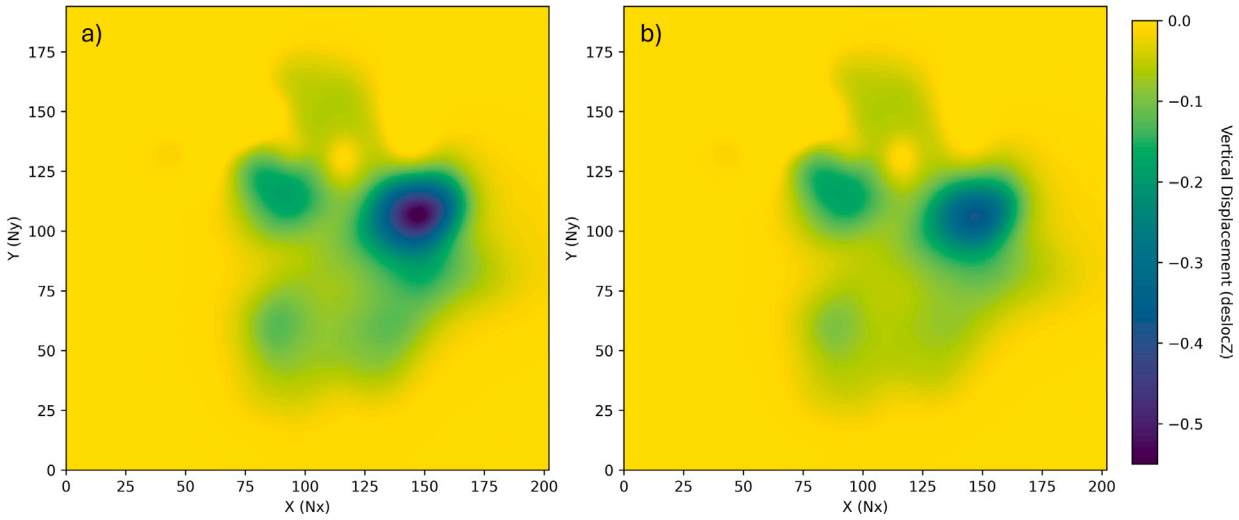


Fig. 11. Comparison of subsidence predictions: (a) subsidence estimated using the detailed model with explicit representation of individual channel architectures, and (b) subsidence estimated using the simplified model parameterized by effective bulk properties inferred from shale content.

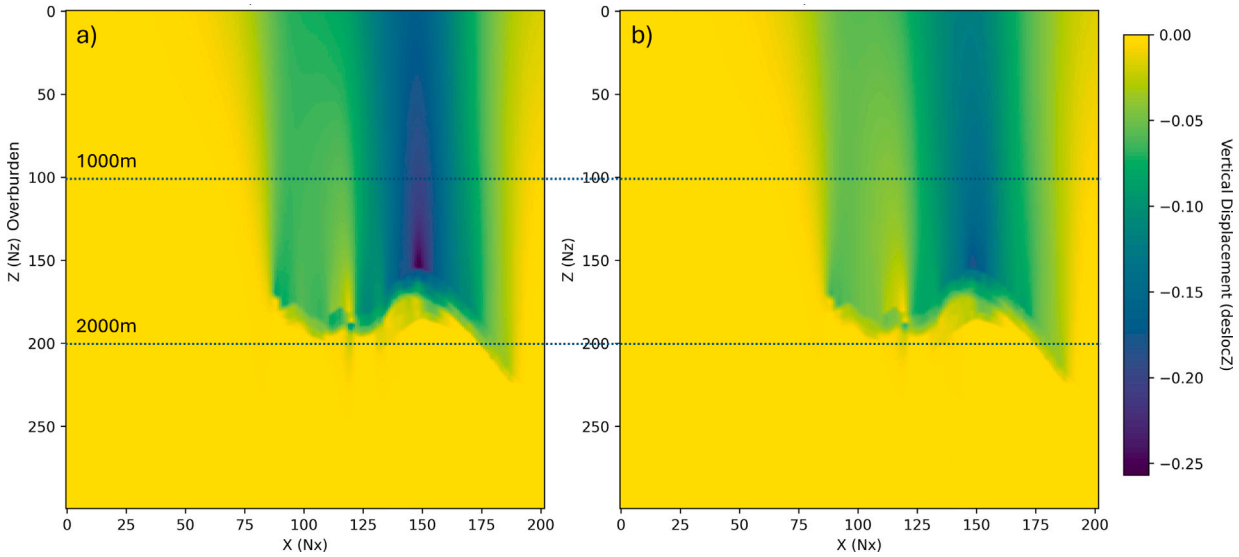


Fig. 12. Cross-sections of the vertical component of displacement (u_{zz}) for (a) the detailed model explicitly representing channel geometries with different mechanical properties assigned to each facies type and for (b) the simplified model using bulk properties derived from the reservoir shale content. The effective Young's modulus is assigned according to the correlation Eq. (11).

well within the uncertainty range of other input parameters, such as pressure depletion magnitudes or baseline mechanical properties. This illustrates the case that a simplified geomechanical approach is sufficient in the early stages of field development and that a complex routine of seismic mapping and geological modeling may not be necessary to infer compaction.

5. Discussion

Our results demonstrate that shale content is the dominant factor controlling effective Young's modulus in channelized reservoir systems, with channel geometry (width and thickness) having minimal impact. The statistical analysis reveals that a model based primarily on shale fraction can predict effective Young's modulus with high accuracy (R^2 = 0.972 for the multivariate regression), while channel geometry parameters together contribute less than 5% to the prediction.

This finding is consistent with the theoretical understanding of composites with strong property contrasts. In our models, sand is the softer (more compliant) phase at 5 GPa, while shale is the stiffer phase at 20 GPa. This assignment reflects the rock physics of deep-water turbidites, where high-porosity reservoir sands have lower stiffness than the surrounding compacted shales.[29–31] When such a contrast exists, the volume fraction of each phase becomes the primary control on effective stiffness, as predicted by mixing laws and effective medium theory.[36]

The field-scale modeling results further support this conclusion, showing that simplified models based on bulk shale content produce compaction and subsidence predictions that are remarkably similar to those from detailed models with explicit channel representation. Two distinct metrics quantify the accuracy of the simplified approach: (1) the regression model for E_{eff} (Eq. (11)) predicts the numerically computed effective modulus with a typical error of less than 10% (maximum relative error across all 100 realizations); and (2) the field-scale maximum subsidence predicted by the homogenized model differs from the heterogeneous model by less than 5% on average, with local deviations up to approximately 10% in areas of strong lithological contrast. Both metrics demonstrate that the simplified approach is sufficiently accurate for engineering purposes.[4]

These findings have important practical implications. First, they suggest that geomechanical assessment can be performed much earlier in field development, even when detailed channel characterization is unavailable. This enables better integration of geomechanical considerations in initial field planning, potentially improving decision-making and risk assessment. Second, resources can be focused on accurately determining bulk compositional parameters (particularly shale content) rather than detailed mapping of channel geometries for geomechanical purposes. Third, the reduced computational requirements of simplified models allow for the exploration of a wider range of scenarios, making uncertainty analysis more tractable.

5.1. Limitations and applicability

Several limitations should be considered when applying the findings of this study. First, the analysis is based on linear elastic constitutive behavior; reservoirs exhibiting significant plastic deformation, creep, or pore collapse (such as North Sea chalk fields) require elasto-plastic or viscoplastic models.[6,7] Second, the uniaxial strain assumption is appropriate for laterally extensive reservoirs but may not hold near field boundaries, faults, or where significant lateral heterogeneity exists. Third, we have not considered mechanical anisotropy, which may be important in thinly laminated sequences where the Backus average differs between vertical and horizontal loading directions.[36]

Fourth, the study focuses on field-scale compaction and subsidence; local phenomena such as wellbore stability, perforation breakdown, casing shear at sand–shale interfaces, or fault reactivation may require detailed representation of heterogeneity and stress concentrations.[2] Fifth, while our synthetic models span a representative range of channel architectures, specific geological settings (e.g., highly amalgamated channels, thick levee sequences) may exhibit different sensitivities. Finally, time-dependent effects such as pressure diffusion and delayed compaction are not addressed here but may be significant over production timescales in low-permeability formations.[1]

Despite these limitations, our simplified approach is well-suited for early-stage field development when detailed geological models are unavailable and rapid scenario evaluation is needed. It provides a first-order estimate of compaction and subsidence that can guide preliminary facilities design and risk assessment, to be refined with more detailed models as field characterization matures.

6. Conclusions

Through a comprehensive analysis of an ensemble of synthetic channel models and field-scale geomechanical simulations, this study addressed the question of how much geological detail is necessary for the accurate prediction of compaction and subsidence in channelized reservoirs. Our main findings are:

1. Shale content is the dominant factor controlling effective Young's modulus in channelized systems, explaining approximately 93% of the variation in our models, while channel geometry (width and thickness) together contribute less than 5% to the prediction.
2. Field-scale simulations show that simplified models based on bulk shale content produce compaction and subsidence predictions that differ by less than 5% on average from detailed models with explicit channel representation.
3. The simplified modeling approach offers significant computational advantages, with run times typically 10 to 30 times faster than detailed models, allowing for more rapid assessment and iteration during early field development.
4. These findings enable geomechanical assessment to be performed much earlier in field development, even when detailed channel characterization is unavailable, potentially improving decision-making and risk assessment.

In conclusion, for the purposes of field-scale compaction and subsidence prediction in channelized reservoirs, detailed representation of channel geometries is unnecessary; a simplified approach based on bulk shale content is sufficient. This finding has significant practical implications for the timing and complexity of geomechanical assessments in field development planning.

CRediT authorship contribution statement

João Paulo Pereira Nunes: Writing – original draft, Software, Methodology, Investigation, Formal analysis, Data curation, Conceptualization. **Gabriel Serrão Seabra:** Writing – original draft, Software, Methodology, Investigation, Formal analysis, Data curation, Conceptualization.

Declaration of competing interest

The authors declare that they have no known competing financial interests or personal relationships that could have appeared to influence the work reported in this paper.

Acknowledgments

The authors thank Petrobras for the permission to publish this work. We also thank Math2Market for their assistance in automating the simulations.

Data availability

The data that has been used is confidential.

References

1. Nagel NB. Compaction and subsidence issues within the petroleum industry: From Wilmington to Ekofisk and beyond. *Phys Chem Earth Part A*. 2001;26(1–2):3–14. http://dx.doi.org/10.1016/S1464-1895(01)00015-1.
2. Bruno MS. Subsidence-induced well failure. *SPE Drill Eng*. 1992;7(2):148–152. http://dx.doi.org/10.2118/20058-PA.
3. Geertsma J. Land subsidence above compacting oil and gas reservoirs. *J Pet Technol*. 1973;25(6):734–744. http://dx.doi.org/10.2118/3730-PA.
4. Settari A, Walters DA. Advances in coupled geomechanical and reservoir simulation with applications to reservoir compaction. *SPE J*. 2001;6(3):334–342. http://dx.doi.org/10.2118/74142-PA.
5. Fjær E, Holt RM, Horsrud P, Raaen AM, Risnes R. Petroleum related rock mechanics. Elsevier; 2021. In: Developments in Petroleum Science; http://dx.doi.org/10.1016/B978-0-12-822195-2.00021-8.
6. Angus DA, Verdon JP, Fisher QJ, Kendall JM. Exploring trends in microcrack properties of sedimentary rocks: An audit of dry-core velocity-stress measurements. *Geophysics*. 2015;80(1):D33–D48. http://dx.doi.org/10.1190/geo2014-0195.1.
7. De Gennaro V, Delage P, Cui YJ, Schroeder C, Collin F. Time-dependent behaviour of oil reservoir chalk: A multiphase approach. *Soils Found*. 2003;43(4):131–147. http://dx.doi.org/10.3208/sandf.43.4_131.
8. van Thienen-Visser K, Breunese JN. Induced seismicity of the groningen gas field: History and recent developments. *Lead Edge*. 2017;36(9):764–770. http://dx.doi.org/10.1190/tle36090764.1.
9. Ward NI, Alves TM, Blenkinsop TG. Differential compaction over late miocene submarine channels in SE Brazil: Implications for trap formation. *GSA Bull*. 2017;130(1–2):208–221. http://dx.doi.org/10.1130/B31510.1.
10. Prather BE, Booth JR, Steffens GS, Craig PA. Classification, lithologic calibration, and stratigraphic succession of seismic facies of intraslope basins, deep-water gulf of Mexico. *AAPG Bull*. 1998;82(5A):701–728. http://dx.doi.org/10.1306/1D9BC48A-172D-11D7-8645000102C1865D.
11. Settari A, Al-Ruwaili K, Sen V. Upscaling of geomechanics in heterogeneous compacting reservoirs. In: *SPE Reservoir Simulation Symposium*. Society of Petroleum Engineers; 2013 http://dx.doi.org/10.2118/163641-MS, Paper SPE-163641-MS.
12. Pereira Nunes JP, Seabra GS, de Sousa LC. A review of CO2-injection projects in the Brazilian pre-salt — Storage capacity and geomechanical constraints. *Int J Greenh Gas Control*. 2024;137:104232. http://dx.doi.org/10.1016/j.ijggc.2024.104232, URL: https://www.sciencedirect.com/science/article/pii/S1750583624001750,
13. Doornhof D, Kristiansen T, Nagel N, Patillo P, Sayers C. Compaction and subsidence. *Oilfield Rev*. 2006;18.

14. Segall P, Fitzgerald SD. A note on induced stress changes in hydrocarbon and geothermal reservoirs. *Tectonophysics*. 1998;289(1):117–128. http://dx.doi.org/10.1016/S0040-1951(97)00311-9, URL: https://www.sciencedirect.com/science/article/pii/S0040195197003119,
15. Fjær E, Holt RM, Horsrud P, Raaen AM, Risnes R. Chapter 12 - reservoir geomechanics. In: *Petroleum Related Rock Mechanics*. Elsevier; 2021:601–662. In: Developments in Petroleum Science; vol. 72, http://dx.doi.org/10.1016/B978-0-12-822195-2.00021-8, URL: https://www.sciencedirect.com/science/article/pii/B9780128221952000218.
16. Avseth P, Mukerji T, Mavko G. *Quantitative Seismic Interpretation: Applying Rock Physics Tools to Reduce Interpretation Risk*. Cambridge University Press; 2005.
17. Walsh JB. Subsidence above a planar reservoir. *J Geophys Res: Solid Earth*. 2002;107(B12):2202. http://dx.doi.org/10.1029/2001JB000606.
18. Skadberg MW. *Spatial Variation in the Overburden R Factor at the Ekofisk Field from 4D Seismic Analysis and Geomechanical Modelling* [Master's thesis]. Trondheim, Norway: Norwegian University of Science and Technology (NTNU); 2017.
19. Taherynia MH, Fatemi Aghda SM, Ghazifard A. Modeling of land subsidence in the South Pars gas field, Iran. *Int J Geosci*. 2013;4:1095–1100. http://dx.doi.org/10.4236/ijg.2013.47103.
20. Mehrabian A, Abousleiman YN. Geertsma's subsidence solution extended to layered stratigraphy. *J Pet Sci Eng*. 2015;130:68–76. http://dx.doi.org/10.1016/j.petrol.2015.03.007.
21. Tempone P, Fjær E, Landrø M. Improved solution of displacements due to a compacting reservoir over a rigid basement. *Appl Math Model*. 2010;34(11):3352–3362. http://dx.doi.org/10.1016/j.apm.2010.02.025.
22. Chen Y, Lizárraga JJ, Buscarnera G. Regional subsidence analysis through a multiscale modeling framework based on breakage mechanics. *J Geophys Res: Solid Earth*. 2021;126(5). http://dx.doi.org/10.1029/2020JB021335, e2020JB021335.
23. Vasco DW, Ferretti A, Novali F. Reservoir monitoring and characterization using satellite geodetic data: Interferometric synthetic aperture radar observations from the Krechba field, Algeria. *Geophysics*. 2008;73(6):WA113–WA122. http://dx.doi.org/10.1190/1.2981184.
24. Liu Y, Helm DC. Inverse procedure for calibrating parameters that control land subsidence caused by subsurface fluid withdrawal: 1. Methods. *Water Resour Res*. 2008;44(7):W07423. http://dx.doi.org/10.1029/2007WR006605.
25. De Waal JA, Smits RMM. Prediction of reservoir compaction and surface subsidence: Field application of a new model. *SPE Form Eval*. 1988;3(2):347–356. http://dx.doi.org/10.2118/14214-PA.
26. Eshelby JD. The determination of the elastic field of an ellipsoidal inclusion, and related problems. *Proc R Soc Lond Ser A. Math Phys Sci*. 1957;241(1226):376–396. http://dx.doi.org/10.1098/rspa.1957.0133, URL: https://royalsocietypublishing.org/doi/abs/10.1098/rspa.1957.0133.
27. Eshelby JD. The elastic field outside an ellipsoidal inclusion. *Proc R Soc Lond Ser A. Math Phys Sci*. 1959;252(1271):561–569. http://dx.doi.org/10.1098/rspa.1959.0173, URL: https://royalsocietypublishing.org/doi/abs/10.1098/rspa.1959.0173.
28. Mavko G, Mukerji T, Dvorkin J. *The Rock Physics Handbook: Tools for Seismic Analysis of Porous Media*. second ed. Cambridge University Press; 2009.
29. Marion D, Nur A, Yin H, Han Dh. Compressional velocity and porosity in sand-clay mixtures. *Geophysics*. 1992;57(4):554–563. http://dx.doi.org/10.1190/1.1443269.
30. Khadem B, Saberi MR, Avseth P. Rock physics of sand–shale mixtures: Classifications, theoretical formulations and study on real dataset. *Mar Pet Geol*. 2021;134:105366. http://dx.doi.org/10.1016/j.marpetgeo.2021.105366.
31. Grochau MH, Gurevich B. Comparison of Gassmann and patchy-saturation theories for time-lapse seismic modeling: a petro-physical perspective. *Geophys Prospect*. 2009;57(4):603–612. http://dx.doi.org/10.1111/j.1365-2478.2009.00800.x.
32. Oliveira RM, da S. Ribeiro NM, Johann PRS, et al. Using seismic attributes to estimate net thickness in pinch–out areas – marlim deep water turbidite oilfield, campos basin. In: *SPE Latin American and Caribbean Petroleum Engineering Conference*. SPE; 2005 http://dx.doi.org/10.2118/94913-MS, SPE–94913–MS.
33. Grochau M, Gurevich B. *Effect of Net to Gross on Time-Lapse Seismic Response in Campos Basin, Brazil*. European Association of Geoscientists & Engineers; 2009 http://dx.doi.org/10.3997/2214-4609-pdb.195.1400_evt_6year_2009, URL: https://www.earthdoc.org/content/papers/10.3997/2214-4609-pdb.195.1400_evt_6year_2009.
34. Pereira Nunes JP, Sebastião Dos Santos M, Maciel N, Davolio A, Formento JL. *Separation of Pressure and Saturation Effects Using Avo 4D in Marlim Field*. European Association of Geoscientists & Engineers; 2009 http://dx.doi.org/10.3997/2214-4609-pdb.195.1508_evt_6year_2009, URL: https://www.earthdoc.org/content/papers/10.3997/2214-4609-pdb.195.1508_evt_6year_2009.
35. Dou L, Chen J, Zuo X, et al. Comparison of mechanical characteristics of different types of shales in the Ordos basin. *Front Earth Sci*. 2023;11:1242567. http://dx.doi.org/10.3389/feart.2023.1242567.
36. Backus GE. Long-wave elastic anisotropy produced by horizontal layering. *J Geophys Res*. 1962;67(11):4427–4440. http://dx.doi.org/10.1029/JZ067i011p04427.
37. Kenny J, Lau D. Small-strain shear modulus of sand–clay mixtures. *Can Geotech J*. 1986;23(1):79–85. http://dx.doi.org/10.1139/t86-010.
38. Bierman S, Marcelis F, Makurat A. Rock physical controls on production-induced compaction in the Groningen gas field. *Sci Rep*. 2018;8:10693. http://dx.doi.org/10.1038/s41598-018-25455-z.
39. Deutsch CV, Tran TT. FLUVSIM: A program for object-based stochastic modeling of fluvial depositional systems. *Comput Geosci*. 2002;28(4):525–535. http://dx.doi.org/10.1016/S0098-3004(01)00075-9.
40. Math2Market. Geodict. 2025 https://www.math2market.com/.
41. Simm R, Bacon M. *Seismic Amplitude: an Interpreter's Handbook*. Cambridge University Press; 2014.
42. Kabel M, Fliegener S, Andrä H, Schneider M, Wiegmann A. Computation of effective elastic properties of composites based on FFT-methods applied to voxel data. *Comput Mater Sci*. 2015;99:153–167. http://dx.doi.org/10.1016/j.commatsci.2014.11.051.
43. Hill R. The elastic behaviour of a crystalline aggregate. *Proc Phys Soc Sect A*. 1952;65(5):349–354. http://dx.doi.org/10.1088/0370-1298/65/5/307.
44. Breiman L. Random forests. *Mach Learn*. 2001;45(1):5–32.
45. Hastie T, Tibshirani R, Friedman J. *The Elements of Statistical Learning: Data Mining, Inference, and Prediction*. 2nd ed. New York: Springer; 2009.
46. Pedregosa F, Varoquaux G, Gramfort A, et al. Scikit-learn: Machine learning in python. *J Mach Learn Res*. 2011;12:2825–2830.
47. Louppe G, Wehenkel L, Sutera A, Geurts P. Understanding variable importances in forests of randomized trees. *Adv Neural Inf Process Syst*. 2013;26.
48. Fitch PJ, Lovell MA, Davies SJ, Pritchard T, Harvey PK. An integrated and quantitative approach to petrophysical heterogeneity. *Mar Pet Geol*. 2015;63:82–96. http://dx.doi.org/10.1016/j.marpetgeo.2015.02.014, URL: https://www.sciencedirect.com/science/article/pii/S0264817215000434,
49. Yakovenko VM, Rosser Jr JB. Colloquium: Statistical mechanics of money, wealth, and income. *Rev Modern Phys*. 2009;81(4):1703–1725. http://dx.doi.org/10.1103/RevModPhys.81.1703.
50. Lake L, Jensen J. A review of heterogeneity measures used in reservoir characterization. *In Situ*. 1991;15(4):409–440.
51. de Figueiredo MO, de Sousa Junior LC, Rodrigues JR, et al. A parallel viscoplastic multiscale reservoir geomechanics simulator. *Upstream Oil Gas Technol*. 2023;11:100095. http://dx.doi.org/10.1016/j.upstre.2023.100095, URL: https://www.sciencedirect.com/science/article/pii/S2666260423000105,